This is a non-peer reviewed preprint submitted to EarthArXiv.

Assessing vertical accuracy and spatial coverage of ICESat-2 and GEDI spaceborne lidar for creating global terrain models

Maarten Pronk[a,b,*], Hugo Ledoux[b], Marieke Eleveld[a,b]

[a] *Deltares; P.O. Box 177, 2600 MH Delft, The Netherlands*
[b] *TU Delft; P.O. Box 5, 2600 AA Delft, The Netherlands*

Abstract

Digital elevation models (DEMs) are a necessity for modelling many large-scale environmental processes. In this study, we investigate the potential of two spaceborne lidar altimetry instruments, ICESat-2 and GEDI—with respect to their vertical accuracies and planimetric data collection patterns—as sources for rasterisation towards global DEMs. We validate the terrain measurements of both missions against airborne lidar datasets over three areas in the Netherlands, Switzerland, and New Zealand, and differentiate them using landcover classes. For our experiments, we use three and a half years of ICESat-2 ATL03 data and three years of GEDI L2A data, totalling 113 million measurements. The datasets are filtered using parameter flags provided by the higher-level products, respectively ICESat-2 ATL08 and GEDI L3A. For all areas and land cover classes combined, ICESat-2 achieves a bias of −0.06 m, a MAE of 0.46 m, and a RMSE of 1.39 m. We find that GEDI is less accurate and precise with a bias of 0.45 m, a MAE of 0.98 m and a RMSE of 5.66 m. Measurements in open land cover classes, such as "Cropland" and "Grassland", result in the best precision for both missions. We also find that the slope of the terrain is a major influence on vertical accuracy, and more so for GEDI than ICESat-2, because of its larger horizontal geolocation error. Contrastingly, we find little effect of either beam power or background solar radiation, nor do we find noticeable seasonal effects on accuracy. Furthermore, we investigate the spatial coverage of ICESat-2 and GEDI by deriving a DEM at different horizontal resolutions and latitudes. GEDI has higher spatial coverage than ICESat-2 at lower latitudes due to its beam pattern and lower inclination angle, and a derived DEM can achieve a resolution of 700 m. ICESat-2 only reaches a DEM resolution of 2000 m at the equator but increases to almost 200 m at higher latitudes. When combined, a 500 m resolution DEM can be achieved globally. Our results indicate that both ICESat-2 and GEDI enable accurate terrain measurements anywhere in the world. Especially in data-poor areas—such as the tropics—this has potential for new applications and insights.

Keywords: ICESat-2, ATL03, GEDI, L2A, DTM, lidar, altimetry, validation, laser, terrain, vertical accuracy, spatial coverage, global

1. Introduction

Digital elevation models (DEMs) are a necessity for modelling many large-scale environmental processes with confidence. Yang et al. (2011) give a detailed overview, a few examples are the detection of geological structures (Masoud and Koike, 2011), the analysis of tectonic evolution (Meigs, 2013), the understanding of volcanic processes (Funning et al., 2005), and assessing flood vulnerability (Hooijer and Vernimmen, 2021; Schumann and Bates, 2018). However, as pointed out by Schumann and Bates (2018), current *global* DEMs are often not suitable as input for those tasks. Compared to DEMs acquired with airborne lidar (Mallet and Bretar, 2009), (1) they have larger vertical errors, (2) their resolution is low, and (3) often they represent

*Corresponding author
Email addresses: maarten.pronk@deltares.nl (Maarten Pronk), h.ledoux@tudelft.nl (Hugo Ledoux), marieke.eleveld@deltares.nl (Marieke Eleveld)

the digital surface model (DSM; vegetation and man-made structures are present) of an area instead of the terrain. These inherent issues stem from the measurement methods used by global DEMs—either interferometry using C-band and X-band radar (SRTM, Tandem-X) or stereoscopy using passive optical imagery (ASTER, ALOS)—to measure elevation (Moudry et al., 2018); lidar can penetrate canopy.

In this study, we investigate an alternative to interferometry/stereoscopy to model global DEMs: spaceborne lidar altimetry. We assess whether, and to what extent, the measurements from two recently launched instruments can be used—based on their vertical accuracy and spatial coverage—as a basis to reconstruct global DEMs. These two instruments are: (1) ICESat-2, which is in a polar orbit to investigate ice sheets (Markus et al., 2017; Neuenschwander and Pitts, 2019), but it also measures canopy height (Neuenschwander and Pitts, 2019); and (2) GEDI, which is attached to the ISS and whose goal is to investigate global ecosystems (Schneider et al., 2020; Dubayah et al., 2020). We further describe these two instruments, and their products (which range from raw measurements, aggregate and gridded products, and derived properties), in Section 2. While these two instruments have been primarily designed for other uses than terrain modelling, it is possible to use them for modelling terrains. For instance, for ICESat-2, Neuenschwander et al. (2020) report a 0.53 m Mean Absolute Error (MAE) and 0.73 m Root Mean Square Error (RMSE) in validating 193 ICESat-2 satellite overpasses in Finland, Malambo and Popescu (2021) report a MAE of 1.20 m for different biomes in the USA, and Wang et al. (2019) report a RMSE of 1.96 m for terrain heights from unclassified ICESat-2 ATL03 product by applying the noise filter proposed by (Zhu et al., 2018). As for GEDI, it has been used less for terrain applications. A validation study with reference areas in Germany by Adam et al. (2020), using the GEDI L2A product (version 1), shows a Median Absolute Deviation (MAD) of 3.42 m, but it should be noted that 2 out of 19 orbits used showed a significant increase in error metrics that they could not account for. Quiros et al. (2021) found a 6.05 m RMSE for terrain heights of the GEDI (L2A, version 1) product in southwest Spain. They also found that by—accounting for the geolocation error—moving the footprints 10 m to the west the results were improved. The study by Zhao et al. (2022) found a horizontal geolocation error of 1.7 m for ICESat-2. Liu et al. (2021) was the first to combine both GEDI (L2A, version 2) and ICESat-2 (ATL08, version 4) in a validation study of 7000 km^2, finding respectively a RMSE of 4.03 m and 2.24 m. More recently, Urbazaev et al. (2022) also combined GEDI (L2A, version 2) and ICESat-2 (ATL08, version 5) in a large validation study, finding a bias of less than a metre for both on their own. Because of their good vertical accuracy, GEDI and ICESat-2 can be used to correct global DEMs, see for instance (Magruder et al., 2021; Hengl et al., 2020; Okolie and Smit, 2022).

It should be noted however that in order to reconstruct a terrain from altimetry observations, more than a good vertical accuracy is required: a good density of observations on the surface of the Earth is also necessary, so that spatial interpolation can be performed. This has however been studied less. As can be seen in Figure 1, both satellites reach their highest density of ground tracks at their inclination angle, but are least dense on the equator. ICESat-2 has been used to generate coarse resolution terrain models, one for Antarctica (Shen et al., 2021) covering 72% of the 1 km grid and a global lowland terrain model at ±1 km (Vernimmen and Hooijer, 2023). GEDI has not been used for the generation of global DEMs yet, not on its own nor in combination with ICESat-2. In the future, both the ICESat-2 and GEDI teams plan to produce 1 km, or coarser, raster products (respectively for level 3 and level 3B (ATL 18)). For example, the GEDI team has already published the 1 km resolution L3 Gridded Land Surface Metrics product (Dubayah et al., 2021b), but not all cells are filled. Notably, these resolutions are an order of magnitude lower than the along-track resolution of ICESat-2 or GEDI. The *possible* resolution of a global DEM based on ICESat-2 and/or GEDI data has not yet been studied.

In this study, we validate the altimetric measurements of both ICESat-2 and GEDI to reconstruct terrains by comparing them against airborne lidar measurements of three locations representing different terrain types (the Netherlands, Switzerland, and New Zealand). To our knowledge, by using reference data from several countries, we present the most representative and extensive validation study (using over 113 million samples) for these datasets thus far. Unlike previous studies, we use the lowest possible level of the products (we do not use aggregates or gridded samples). Furthermore, unlike previous studies, we assess the density of samples in the planimetric direction for large areas ranging from the equator to the poles, which allows us to identify which resolutions of a (global) DEM could be achieved. Also, we consider and

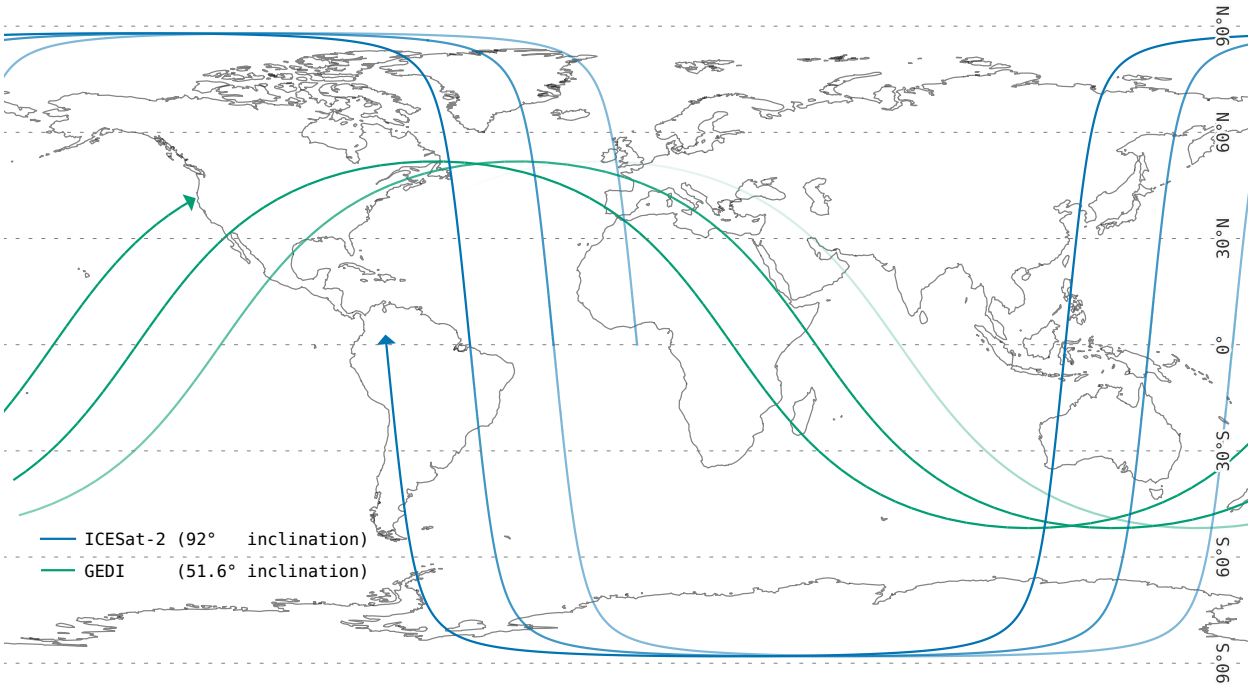

Figure 1: Ground tracks for three successive orbits of ICESat-2 and GEDI. The satellite is represented by a triangle and past orbits fade out. Note the increased density of ground tracks at the latitude of inclination, as well as the lack of coverage beyond 51.6° latitude for GEDI.

study other factors that can influence the quality of the altimetric measurements: strong/weak beams, day/nighttime, terrain slope, seasonal effects and the presence of water. Our final results allow practitioners to make informed decisions, such as choosing to filter certain ground tracks that contain mostly outliers.

2. Datasets & Methods

2.1. ICESat-2 and GEDI

The Low-Earth Orbit (LEO) of ICESat-2 at an orbit inclination of 92°, covers the earth between −88° and 88° latitude. Its lasers split into six beams, divided into three pairs, each pair 90 m apart and the pairs 3.3 km apart, for a total swath width of 6.6 km. Each pair contains a strong beam (175 μJ) and a weak beam (45 μJ), with a power ratio of 4:1 (Markus et al., 2017). Along-track, it can measure every 0.7 m, while its beam footprint is ±17 m, thus consecutive measurements overlap.

The orbit of GEDI, itself attached to the Japanese Experiment Module at the International Space Station (ISS), is between 51.6° N and 51.6° S. Its sensor has eight beams, each 600 m apart, for a total swath width of 4.2 km. Of the eight beams, four are strong (10 500 μJ) while the other four are weak beams (4200 μJ), with a power ratio of 2.5:1 (Wake et al., 2019). GEDI measures a point every 70 m along-track, with a beam footprint of 23 m.

Both missions have multiple laser beams and a division in beam energy, resulting in weak and strong beams. Weak beams (or coverage beams) are a way to improve coverage while still maintaining the mission requirement(s) for a specific power level with the strong beams. Coverage is further increased for both missions by the ability to angle the instruments away from their reference ground tracks (Neuenschwander and Pitts, 2019; Dubayah et al., 2020), preventing repetitions of the same ground track. The characteristics of both missions are summarised in Table 1.

Table 1: Key characteristics of GEDI and ICESat-2 missions in comparison with a typical airborne mission.

Mission	ICESat-2	GEDI	Airborne lidar
Type	Discrete photon	Full waveform	Either
Objective	Cryosphere monitoring	Ecosystems	-
Duration	2018–2023	2019–2023	Single flight(s)
Orbit Inclination	92°	51.6°	NA
Laser pulse power	1x 660 μJ	3x 10 500 μJ	200 μJ to 8000 μJ
Beam power (strong/weak)	175 μJ/45 μJ	10 500 μJ/4200 μJ	200 μJ to 8000 μJ
# beams	6 (in 3 strong/weak pairs)	8 (four strong, four weak)	1
Elevation	±480 km	±420 km	0.5 km
Beam footprint	17 m	23 m	0.05 m
Along track spacing	0.7 m	70 m	0.1 m
Across track spacing	3 km/90 m between pair	0.6 km	0.1 m
Swath width	6.6 km	4.2 km	1 km
Beam frequency	512 nm (green)	1064 nm (near-infrared)	Either

The data from the ICESat-2 and GEDI missions are made publicly available in several data products, categorised in subsequent Level 1, 2, and 3 data products. Level 1 products contain the raw telemetry, whereas Level 2 products contain directly usable geolocated data to which several corrections—such as accounting for atmospheric effects—are applied. Data for Level 3 are aggregated versions of Level 2 products, which are smaller in filesize and easier to process. ICESat-2 differentiates between a Level 3A, which aggregates consecutive samples along the ground track of Level 2 data products, and a Level 3B, which are gridded versions of the aggregated Level 3A data products. GEDI's Level 3 data product are gridded versions of Level 2 data products, like ICESat-2's Level 3B.

Both missions make their data available online in *granules*, which are subsections of a single orbit. GEDI divides one orbit into 4 granules (but only since version 2), while ICESat-2 has 15 granules per orbit. The Land Processes (LP) Distributed Active Archive Center (DAAC) distributes the GEDI L2A data, while the National Snow and Ice Data Center (NSIDC) DAAC distributes ICESat-2 data.

We used the ICESat-2 Level 2 ATL03 product (Neumann et al., 2021), currently at version 5, with dates ranging from 2018-10-13 to 2022-04-04. This dataset is not classified, so we used the classification *signal_photons/classed_pc_flag* flag from the higher Level 3 ATL08 product (Neuenschwander et al., 2021) to classify each photon. These classifications include "noise", "ground", "canopy" and "top of canopy", of which we only use "ground". For elevation, we used the *heights/h_ph* (height photon) containing the elevation above the WGS84 ellipsoid and related latitude *heights/lat_ph* and longitude *heights/lon_ph* for each track group in the HDF5 file. We did not apply further filtering but noted that classified points ordinarily have a confidence level of 3 (medium) or 4 (high), thereby filtering out lower confidence values.

To investigate the performance of GEDI, we used the GEDI L2A data product (Dubayah et al., 2020, 2021a) at version 2. As of writing, this covers dates from 2019-04-18 to 2022-03-16. For elevation, we used the *elev_lowestmode* field and related latitude *lat_lowestmode* and longitude *lon_lowestmode* fields for each track group in the HDF5 file. We filtered the data based on the settings that are used to produce the higher level L3A (version 2) product (Dubayah et al., 2021c), which uses points from the L2A product in a sparse 1 km resolution raster product. These settings only include data with the flags *rx_assess_quality_flag* set to non-zero, *surface_flag* set to non-zero and *degrade_flag* set to zero, with all flags specified in Appendix A.

2.2. Reference datasets: airborne lidar and land cover

We compared ground elevation points from both missions with terrain reference datasets based on airborne lidar. Areas included are the Netherlands, Switzerland, and New Zealand, for a total of 25 663 km^2. These datasets cover flat to steep terrain and several forest types in different climate zones in the world. Note that GEDI doesn't cover the full area of the Netherlands.

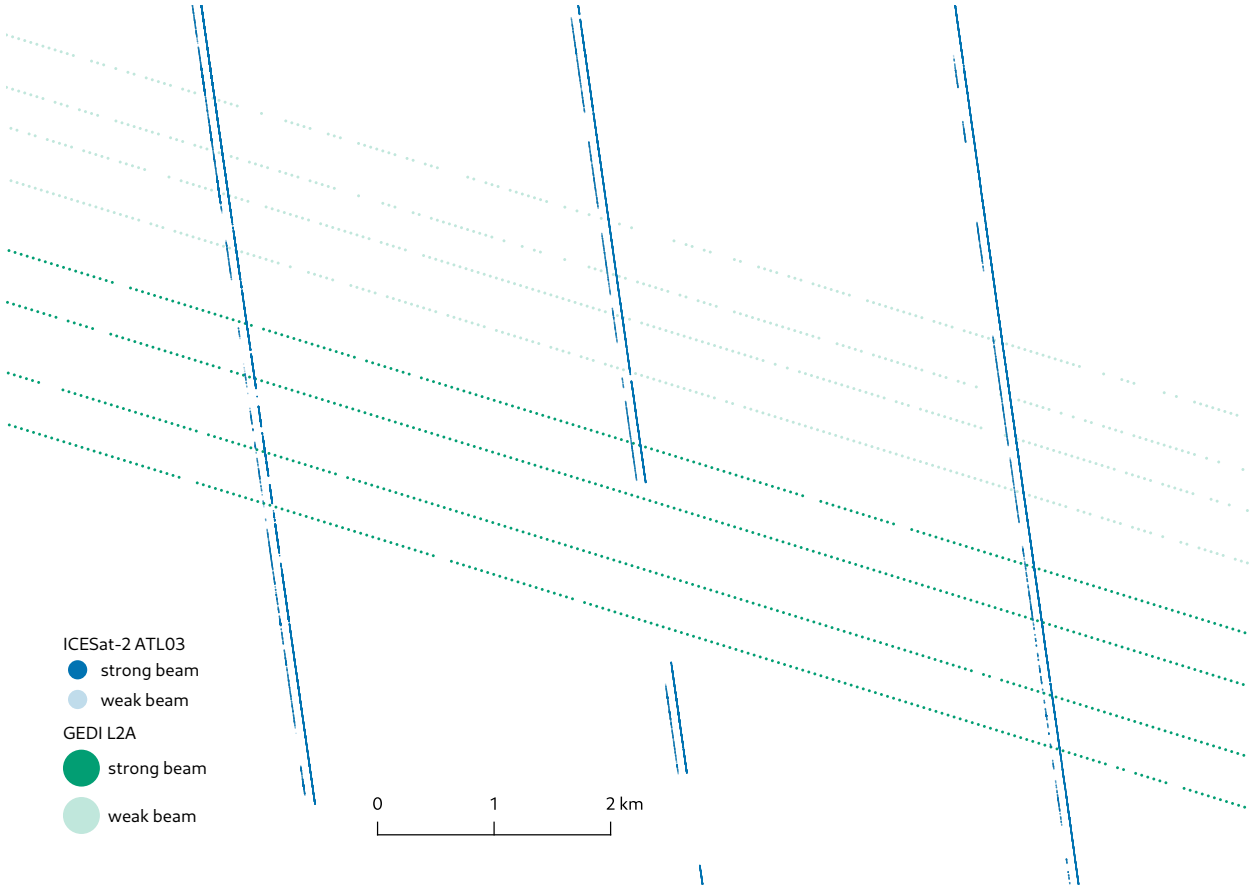

Figure 2: Filtered ICESat-2 ATL03 (blue) and GEDI L2A (green) points from a single granule each at the 47th latitude to scale, demonstrating the beam patterns. Note that ICESat-2 has a smaller beam footprint and a much higher pulse repetition, but a more uneven spatial coverage than GEDI. The gaps between data here will decrease by using multiple granules, but will never disappear completely.

The validation dataset used for the Netherlands is the 5 m DTM version of the AHN4 (2020–2021), sourced from `https://www.ahn.nl/ahn-viewer`. Referencing to the ellipsoid was conducted with the pipeline described with RDNAPTRANS2018, requested from `https://www.nsgi.nl/geodetische-infrastructuur/coordinatentransformatie`. While the AHN4 is not complete over the northern part of the Netherlands (only relevant for ICESat-2), it overlaps in time with ICESat-2 and GEDI, whereas the previous version of the AHN (version 3; collected between 2013–2018) does not. The validation dataset used for Switzerland is the 0.5 m DTM version of the Kanton Zürich (2017–2018) dataset based on swissSURFACE3D, sourced from the Geographisches Informationssystem des Kantons Zürich (GIS-ZH), the Digitales Terrainmodell (DTM) `https://geolion.zh.ch/geodatensatz/3508`. Referencing to the ellipsoid was conducted by the geoids provided at `https://cms.geo.admin.ch/ogd/geodesy/Geoid_OGD.zip`. The validation dataset used for New Zealand is the 1 m DTM version of the Auckland South lidar (2016-2017) dataset, sourced from the LINZ Data Service (`https://data.linz.govt.nz/`) and licensed for reuse under CC BY 4.0. Referencing to the ellipsoid was conducted by the geoids provided at `https://www.geodesy.linz.govt.nz/download/proj-datumgrid-nz`. An overview is given in Table 2.

Note that airborne lidar datasets differ considerably from spaceborne lidar, most notably so in their platform, resulting in considerable differences in beam footprint and ground coverage (see Table 1). The altitude increase results in a wider beam footprint, from ±0.5 m (at 500 m (van Dijk and Bos, 2013)) for airborne platforms to ±20 m for space platforms. Although much wider, it is a small increase compared to

Table 2: Reference datasets based on airborne lidar with the amount of ICESat-2 and GEDI granules that intersect each area.

Country	the Netherlands	Switzerland	New Zealand
Latitude	50°-53°N	47°N	37°S
Dataset	AHN4	Kanton Zürich	Auckland South
Years collected	2020-2021	2017-2018	2016-2017
Area	21 800 km^2	1728 km^2	2135 km^2
Resolution	5 m	0.5 m	1 m
Uncertainty	<0.1 m	<0.1 m	<0.1 m
Terrain type	Delta	Mountainous	Foothills
Elevation range	0-300 m	350-1300 m	0-700 m
ICESat-2 granules	518	138	135
ICESat-2 size	808 GB	255 GB	113 GB
GEDI granules	1525	190	149
GEDI size	2998 GB	405 GB	187 GB

the increase in sensing altitude, going from 0.5 km to 480 km. Airborne lidar often focuses on maximising coverage (points/m^2) of smaller areas, whereas the coverage for space lasers is the ground track of the satellite. While both ICESat-2 and GEDI employ instruments with multiple (split) laser beams, including the ability to point the laser away from the ground track—all to maximize coverage—this still results in very sparse and uneven coverage as shown in Figure 2. A comparison is given in Table 1.

In order to differentiate the results from the comparison with the reference datasets, we also sampled the land cover class from the ESA WorldCover 2020 dataset (Zanaga et al., 2021). WorldCover recognizes several land cover classes, such as "Grassland", "Cropland", "Tree cover" and "Built-up", that we used to differentiate the error metrics. Only land cover classes accounting for more than 1% of all samples—around 600 000 points—have been taken into account.

An overview of these datasets for the area of New Zealand is given in Figure 3. The overviews for the two other reference areas are in Appendix B.

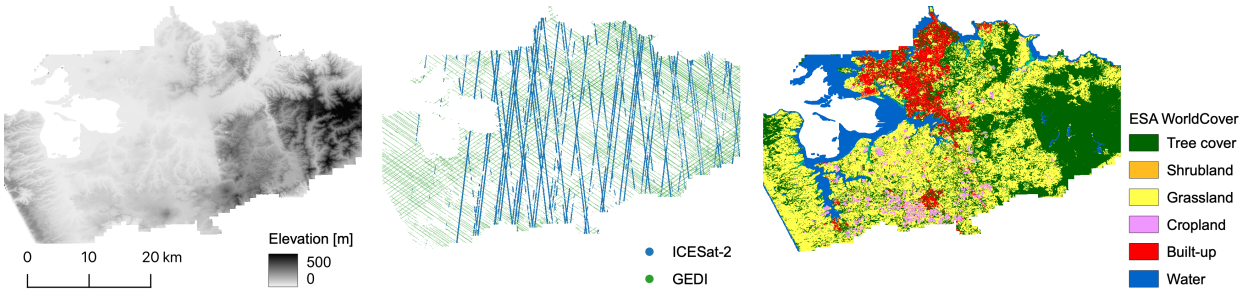

Figure 3: A visual overview of the datasets used for the reference area in New Zealand. On the left is the airborne lidar DTM, in the middle the spaceborne lidar data, and on the right the landcover classes according to ESA WorldCover.

2.3. Methods

This study investigates the vertical accuracy of both ICESat-2 ATL03 and GEDI L2A data by comparing them with DTMs based on airborne lidar in different countries and terrain types. Furthermore, we assess the density of samples in the planimetric direction to identify which resolutions of a (global) DEM based on ICESat-2 and/or GEDI could be achieved. The ATL03 and L2A products, both Level 2 products, are the lowest level or highest resolution data products available for both missions that are geolocated and corrected

for geophysical effects, thus containing directly applicable elevation values. We differ from most studies in using the Level 2 ATL03 data product for ICESat-2, and not its Level 3 ATL08 product, which is a 100 m aggregated version of ATL03.

All granules intersecting with the reference areas were searched using NASA Earthdata Search and downloaded from their archive centres. This download resulted in 2655 granules with a total size of ±4.8 TB, as detailed in Table 2. After data filtering—for both quality and geographic area—data from a remaining 1488 granules (56%) were used.

For each ICESat-2 or GEDI measurement z, we retrieved the corresponding cell values from the reference raster datasets. Given a 5 m resolution reference raster, ICESat-2—with a 17 m footprint—covers roughly 3×3 cells. GEDI, with its slightly larger footprint, would cover 5×5 cells. Our experiments showed there is no discernable difference between sampling the centre cell, the mean or median of all cells. We take the centre cell—the midpoint of the beam—to obtain a single value c which we use in the following metrics:

$$\text{Mean Error (bias)} = \frac{1}{n}\sum_{i=1}^{n} z_i - c_i \tag{1}$$

$$\text{Mean Absolute Error (MAE)} = \frac{1}{n}\sum_{i=1}^{n} |z_i - c_i| \tag{2}$$

$$\text{Root Mean Square Error (RMSE)} = \sqrt{\frac{1}{n}\sum_{i=1}^{n} (z_i - c_i)^2} \tag{3}$$

In order to assess the coverage of ICESat-2 and GEDI—and thus the possible resolution of a (global) DEM based on ICESat-2 and GEDI lidar—we rasterised ICESat-2 and GEDI data into 5 km * 10 km rasters at several resolutions for a range of latitudes. We did so along the 103rd meridian east, as it is one of the few areas which has almost continuous landmass from the 0° latitude onwards. Similar to the procedure followed in assessing the vertical accuracy, all granules intersecting with a bounding box around the 103rd meridian east were downloaded and processed. This download resulted in 41 608 ICESat-2 granules and 6718 granules for GEDI, over 11 TB of data.

We rasterised by counting the samples falling inside each raster cell. Rasterising at a high resolution will thus leave many cells empty, while rasterising at a low resolution will fill up the entire grid with values equal to or larger than one. We denote the ratio of non-zero cells as the *spatial coverage (%)*. At 100%, it gives a lower bound to the density: at least 1 point per cell at a given resolution. Given the possible presence of waterbodies—and thus gaps in the coverage—a 100% spatial coverage is unrealistic. We thus qualify reasonable spatial coverages of 80% and up fit for DEM creation purposes.

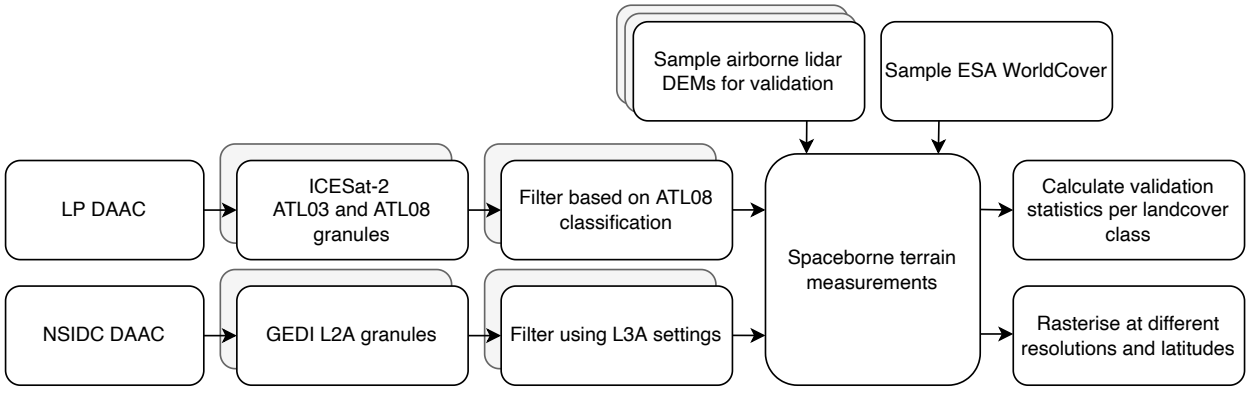

Figure 4: Overview of the datasets and methods used in this study.

An overview of the methods is given in Figure 4. The above-mentioned search, extraction, sampling and rasterisation algorithms have been implemented in the programming language Julia (Bezanson et al., 2017). The code—making use of the the open-source package SpaceLiDAR.jl (Pronk and Gardner, 2021)—and instructions are available at `https://anonymous.4open.science/r/icesat2-gedi-val-dtm`.

3. Results

3.1. Accuracy

Table 3: Validation of ICESat-2 ATL03 and GEDI L2A terrain data with reference areas for each landcover class. n is the number of observations.

Landcover	bias [m]		MAE [m]		RMSE [m]		n	
	ICESat-2	GEDI	ICESat-2	GEDI	ICESat-2	GEDI	ICESat-2	GEDI
Sparse	−0.08	0.21	0.44	1.10	1.29	4.97	2 052 659	62 026
Grassland	−0.19	0.29	0.37	0.83	0.90	5.16	61 161 597	2 288 181
Cropland	−0.04	0.38	0.26	0.64	0.69	4.26	22 693 483	1 855 826
Tree cover	−0.19	0.66	0.56	1.58	1.72	7.47	12 426 471	1 307 163
Built-up	0.98	0.86	1.46	1.29	3.47	6.78	8 924 993	584 001
All landcovers	−0.06	0.45	0.46	0.98	1.39	5.66	107 259 203	6 097 197

When compared with the airborne DTMs across all three validation areas, ICESat-2 achieves a bias of −0.06 m, a MAE of 0.46 m, and a RMSE of 1.39 m (N=107 259 203). GEDI is less accurate with a bias of 0.45 m, a MAE of 0.98 , and a RMSE of 5.66 (N=6 097 197) as demonstrated in Table 3. In this comparison, ICESat-2 has ±19 times as many samples as GEDI, which is less than the expected factor of hundred from their along track spacing specifications. The applied filters thus removed a larger ratio of ICESat-2 samples than from GEDI. The imbalance in the number of samples skews the accuracy in favour of ICESat-2 when all samples are combined, resulting in a bias of −0.02 m, a MAE of 0.49 m, and a RMSE of 1.89 m (N=113 356 400).

Open land cover, such as "Cropland" and "Grassland", result in the best precision for both missions. Precision decreases in "Sparse vegetation" areas and is worst in "Tree Cover" for GEDI and in "Built-up" areas for ICESat-2. Both missions are the least accurate in urban areas, as they mistake buildings for ground, resulting in a strong positive bias of 0.9 m.

In terms of accuracy, ICESat-2 exhibits a small negative bias (which is partially obfuscated by the positive bias in "Built-up" areas). Conversely, GEDI has a larger positive bias. These biases are present and consistent in all validation areas. Separate results for each validation area are provided in Appendix C.

There is a considerable tail present in the distribution of these differences, which is to be expected based on the total number of measurements. In Figure 5, we show the elevation differences with the reference dataset from Table 3. We used so-called boxenplots or letter-value plots to also visualize the (shape of the) tail of these large datasets (Hofmann et al., 2017). Note that ICESat-2 has more negative than positive outliers (a negative skew), while the outliers of GEDI are balanced (zero skew), except in "Built-up" areas.

3.2. Spatial coverage

Figure 6 shows which percentage of cells within a grid intersect with ICESat-2 and GEDI data for multiple resolutions and latitudes on the 103rd meridian east. Note that coverage is decreased over oceans, lakes, and rivers, and that our ATL03 classification with ATL08 excludes polar ice. Near the poles, it is possible to achieve a 200 m resolution with ICESat-2 as roughly 86 % of the cells are filled with at least one data point. Moving towards the equator, with the addition of GEDI from the 51st latitude onwards, the combined achievable resolution is 500 m.

Note that due to the configuration of the ICESat-2 beam pairs (see Figure 2), combined with the high inclination, GEDI achieves a more even sampling density. Indeed, GEDI consistently fills more cells than ICESat-2 in Figure 6, reaching a possible 700 m resolution on its own, whereas ICESat-2 only reaches 2000 m.

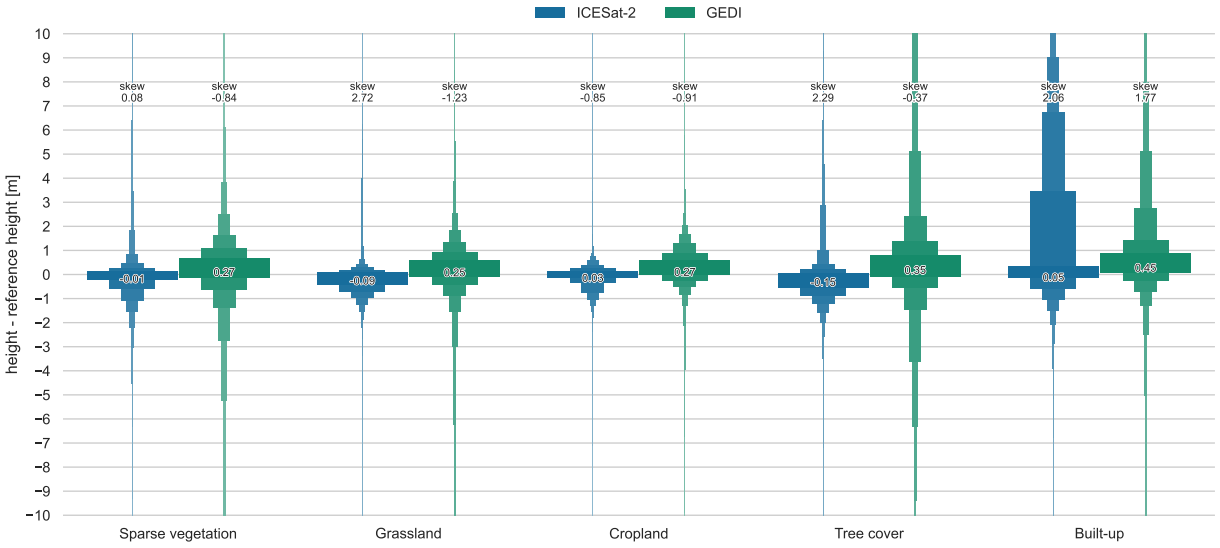

Figure 5: Elevation difference as boxenplots for both missions compared to reference areas per landcover type (ESA Worldcover). The median (centre) and skewness (top) is also given for each boxenplot. ICESat-2 is more precise (MAE 0.46 m) and much more accurate (bias of −0.06 m) than GEDI (MAE 0.99 m and bias of 0.46 m). GEDI performs worst in "Tree cover" areas, while ICESat-2 has the worst precision in "Built-up" areas.

3.2.1. Influence of strong and weak beams

Both ICESat-2 and GEDI have strong and weak beams, and weaker beams are not expected to fully penetrate dense canopy. However, after data filtering, the accuracy for both the strong and weak beams are comparable for both missions, as shown in Figure 7a. The weak beam measurements are only slightly less accurate than those from the strong beam. To achieve this accuracy, we note that the weak beam data only accounts for 20% of the ICESat-2 data, the rest of the data has been filtered out. This effect was already visible in Figure 2. Remarkably, GEDI has a much higher percentage of weak beam data (roughly 50%) and still achieves comparable accuracy to its strong beam. We suspect that this can be explained by the much higher pulse energy of the full-waveform lidar instrument of GEDI compared to single-photon lidar of ICESat-2, combined with the lack of dense (tropical) canopy in our validation areas.

3.2.2. Solar background influence

Lidar instruments, especially those with wavelengths like ICESat-2's green 532 nm, but also GEDI's near-infrared 1064 nm one, are sensitive to background noise from the sun (Thuillier et al., 2003), as their spectra overlap (Neumann et al., 2019). In both cases an additional radiance signal from sunlight will be scattered into the telescope from atmosphere and surface. Therefore, it is expected that measurements made during the day are less accurate than those done during the night. However, as seen in Figure 7b, the results are comparable between daytime and nighttime. We do note however that slightly more data is filtered out for both ICESat-2 and GEDI during the day.

3.2.3. Seasonal influence

In the parts of the world with leaf-on and leaf-off seasons, airborne lidar is often collected during winter to maximize ground returns, as there is less canopy to reflect on. Indeed, the airborne lidar reference datasets from the Netherlands and Switzerland have been collected in winter. However—while there are differences between different months—we find no clear seasonal pattern when the measurements are split for each month of the year (Figure 8), even when only taking the "Tree cover" land cover classification into account.

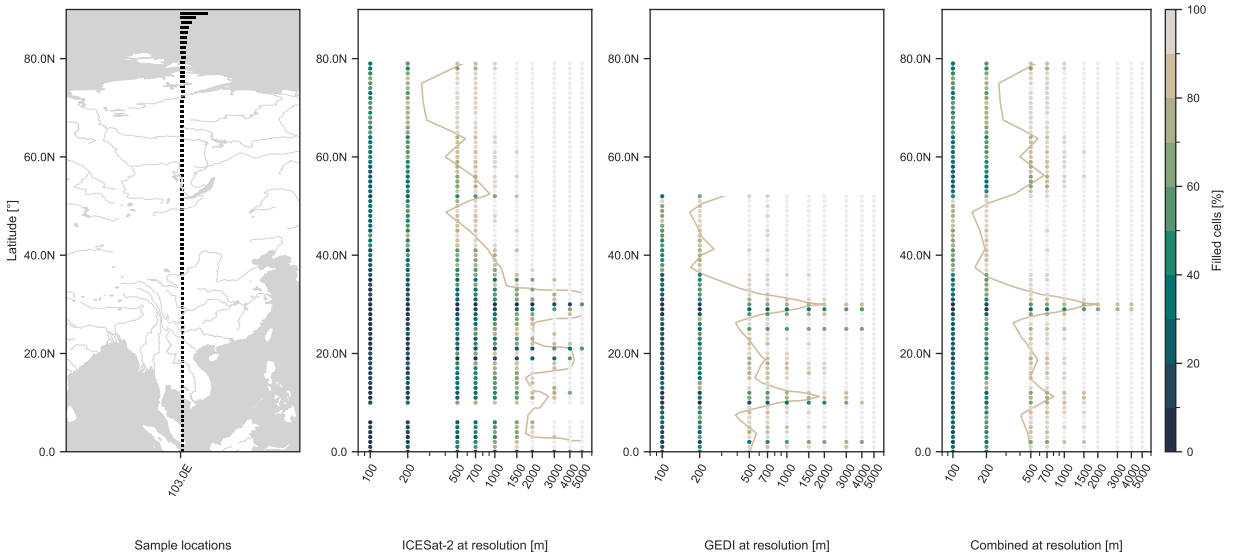

Figure 6: Spatial coverage (% of cells filled) for several grid resolutions at each latitude. A contour line for 80 % is also given. By combining both ICESat-2 and GEDI a 500 m (with >80% filled) resolution DEM is possible. Note that locations over oceans, lakes and rivers have a decreased coverage, and for this longitude there is decreased coverage over the Sichuan Basin (30° N) in China for unknown reasons. The sample locations (5*10 km rasters as black rectangles) appear wider at higher latitudes due to the map projection.

3.2.4. Geolocation accuracy

Depending on the slope of the terrain, horizontal geolocation errors can result in considerable vertical errors. Indeed, slope is one of the major factors influencing the accuracy of lidar (Su and Bork, 2006). This is especially true for spaceborne lidar with much larger geolocation errors and footprints than airborne lidar: a measurement at the edge of ICESat-2's 17 m footprint on a slope of 25 % will result in a vertical error of 4 m compared to a centre measurement.

In Figure 9 we plot the difference between ICESat-2 and GEDI and the reference for different slopes in Switzerland. We observe a clear decrease in both accuracy as precision with slope, and note that for both missions the bias is negatively correlated. However, ICESat-2's accuracy suffers less from slope than GEDI, but both are directly related to their geolocation accuracy. For steeper slopes, little to no skewness is observed. ICESat-2 has a positive skewness on 0° to 10° slopes, due to the presence of urban areas. From these results we estimate a geolocation error of ±4 m for ICESat-2 and ±9 m for GEDI.

3.2.5. Presence of water

The presence of water can result in specular reflections. When combined with the previously discussed beam footprint, the presence of water at the edge of the footprint can thus become the dominant elevation signal. In effect, this widens water bodies with half of the footprint, which is significant (7 m to 8 m) for smaller water bodies such as streams. This phenomenon shows up as negative outliers near (the edge) of water, as shown in Figure 10a.

4. Discussion

4.1. Factors influencing the accuracy

Our results for both ICESat-2 and GEDI are comparable to findings from previous studies—even though the study areas differ. Wang et al. (2019) reported a RMSE of 1.96 m for terrain heights from the unclassified ICESat-2 ATL03 product, compared to our 1.35 m. A better RMSE of 0.75 m was reported by Xing et al. (2020), but with only two beams of single granule their number of samples was limited. The 5.81 m RMSE

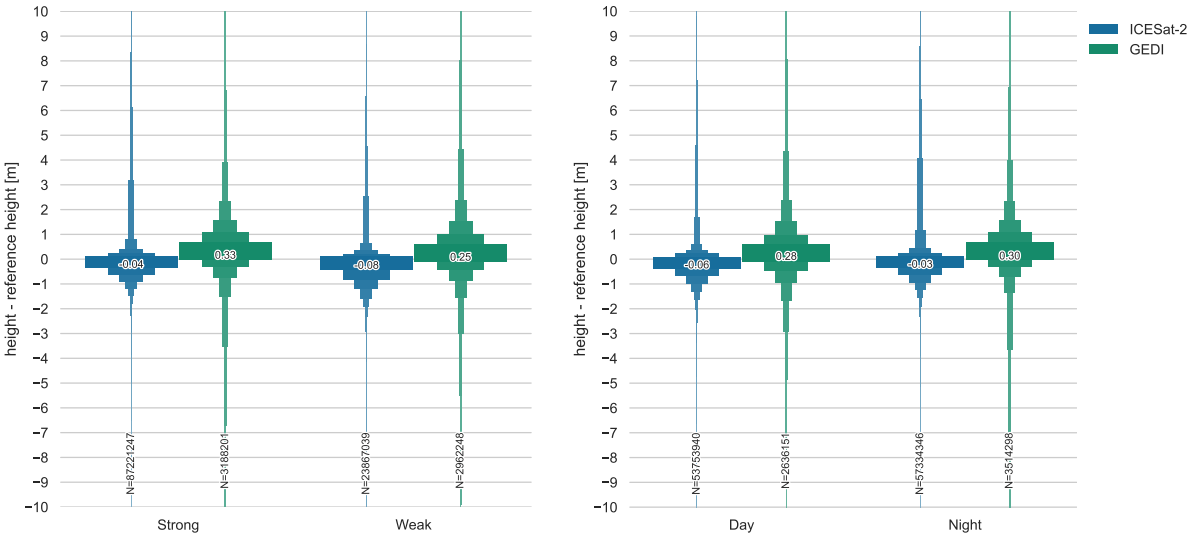

Figure 7: Terrain elevation difference for both missions compared to reference by (a) beam power and (b) time of day. The median, and the number of samples is included in the middle and lower part of the figure, respectively. Overall the results are similar for both comparisons and missions, but note that ICESat-2 filtered much more data from its weak beam than GEDI.

for GEDI found here is comparable to the 6.05 m RMSE found by Quiros et al. (2021) in southwest Spain. Contrastingly, Liu et al. (2021) found a better RMSE of 4.03 m for GEDI than ours, but a worse MAE of 1.80 m (ours 0.99 m) and bias of 0.97 m (ours 0.46 m). We suspect our GEDI data (collected during 2019–2022) contains more outliers due to a different distribution of landcover classes than the data used by Liu et al. (2021) (collected during 2019, with no differentiation per landcover class), which explains the difference in RMSE. Like Urbazaev et al. (2022), we found that ICESat-2 and GEDI both have sub-meter biases. For ICESat-2 these biases can be measured in centimetres, approaching airborne lidar territory.

All reference datasets are based on lidar and have accuracies within ±10 cm. These datasets were collected between 2020–2021 (the Netherlands), 2017–2018 (Switzerland) and 2016–2017 (New Zealand), while ICESat-2 data are from 2018–2022 and GEDI data are from 2019–2022. Some inaccuracies found here—mostly for the urban areas—could thus stem from temporal differences.

4.1.1. Geolocation accuracy

Our estimation a geolocation error of ±4 m for ICESat-2 and ±9 m for GEDI, agree with the 2.5 m–4.4 m geolocation error of ICESat-2 (Luthcke et al., 2021) and the 10 m geolocation error of GEDI (Dubayah et al., 2021a).

Neuenschwander and Magruder (2019) found an increase in vertical accuracy by horizontally offsetting the location by −5 m along track, thereby accounting for possible geolocation errors. We repeat our accuracy measurements in the Swiss reference area—the one with the most relief—with several offsets based on the movement direction of the satellite. The offsets are specified as 2.5 m, 5 m, and 10 m in forward, backward (along-track) and left, right (across-track) directions. However, we find no consistent improvement in accuracy for any of the offsets. For limited selections of steeper slopes, we do find bias improvements by using offsets, but note that these are likely due to a small number of samples in specific terrain. We thus could not replicate the findings of Neuenschwander and Magruder (2019), nor those of Quiros et al. (2021), who found that accuracy for GEDI increased by offsetting the location 10 m to the left. However, we respectively use the version 5 of ICESat-2 ATL03 and version 2 of GEDI L2A in our study (versus version 1—both for ICESat-2 and GEDI—in theirs). GEDI version 2 has significantly improved the geolocation error (Dubayah et al., 2021a), which we confirm here.

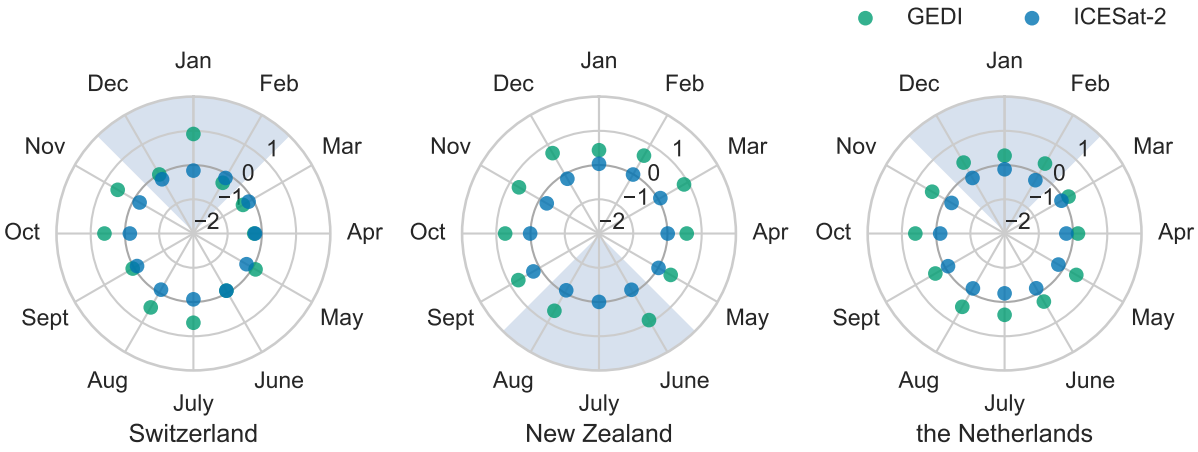

Figure 8: The bias of ICESat-2 and GEDI split out per month and reference area in rose plots. The winter months are shaded in light blue. Note that sometimes there is no GEDI data in a given month.

4.1.2. Outlier tracks

We note that several granules of both ICESat-2 and GEDI missions contain consistent gross outliers. The elevations of these granules are consistently much higher or lower than the reference elevation, often tens of meters. Similarly, Adam et al. (2020) found GEDI granules with significantly higher errors. A timing error in the pipeline is the most likely source of these outliers, as all elevations are offset by roughly the same error, so the terrain profile is present. For ICESat-2 a list of retracted granules was published for version 3 of the data, which have been fixed in subsequent versions. For GEDI no such list exists as of writing, although one is mentioned in the GEDI documentation for Level 3 products.

In this study we have filtered all granules that were consistently 30 m above or below the global reference surface, using the fields (*geophys_corr/dem_h* for ICESat-2 and *digital_elevation_model* for GEDI) present in the data products. Lower thresholds would also filter out correct data. We identified more erroneous granules, especially for GEDI, but found no clear metric to uniquely identify these granules without removing actual data. Our resulting list of unused granules for the reference areas is found in Appendix D.

4.2. Spatial coverage and the resolution of global DEMs

While no global DEM based on GEDI exist as of writing, several have been made using ICESat-2. The 1 km DEM of Antarctica by Shen et al. (2021) could be improved to 200 m by using all ICESat-2 data. The GLL_DTM by Vernimmen and Hooijer (2023) using all ICESat-2 data is already at a 1 km resolution. Adding GEDI data to such DEMs (applicable only between 51.6° N and 51.6° S latitude) would further improve the resolution, but lower the accuracy. This trade-off depends on the slope of the terrain, i.e. whether the error due to the gap in ICESat-2 data is larger than the error due to the lower accuracy of GEDI.

The achievable global DEM resolution of 500 m by combining ICESat-2 and GEDI is still far removed from current available global DEMs at 30 m resolution. However, as pointed out by Bates (2012), current global DEMs measure the elevation of the surface, which is not necessarily the elevation of the terrain. Accurate (airborne) lidar DEMs are currently only available for a small fraction of the globe. Spaceborne lidar DEMs thus are a valuable addition, especially in data-scarce regions with ubiquitous forest cover, such as the tropics, even at a low resolution.

The spatial coverage—after four years of continuous data collection—will still improve during the remaining lifespan of these satellites. GEDI has passed its planned mission duration, and has been put into hibernation on the ISS after an extension of its mission duration. Another extension has been requested (Sidik, 2022) and there are plans to enable GEDI again from 2024 onwards. ICESat-2 has also exceeded its nominal mission duration and could probably continue for another year (into and beyond 2023), given enough

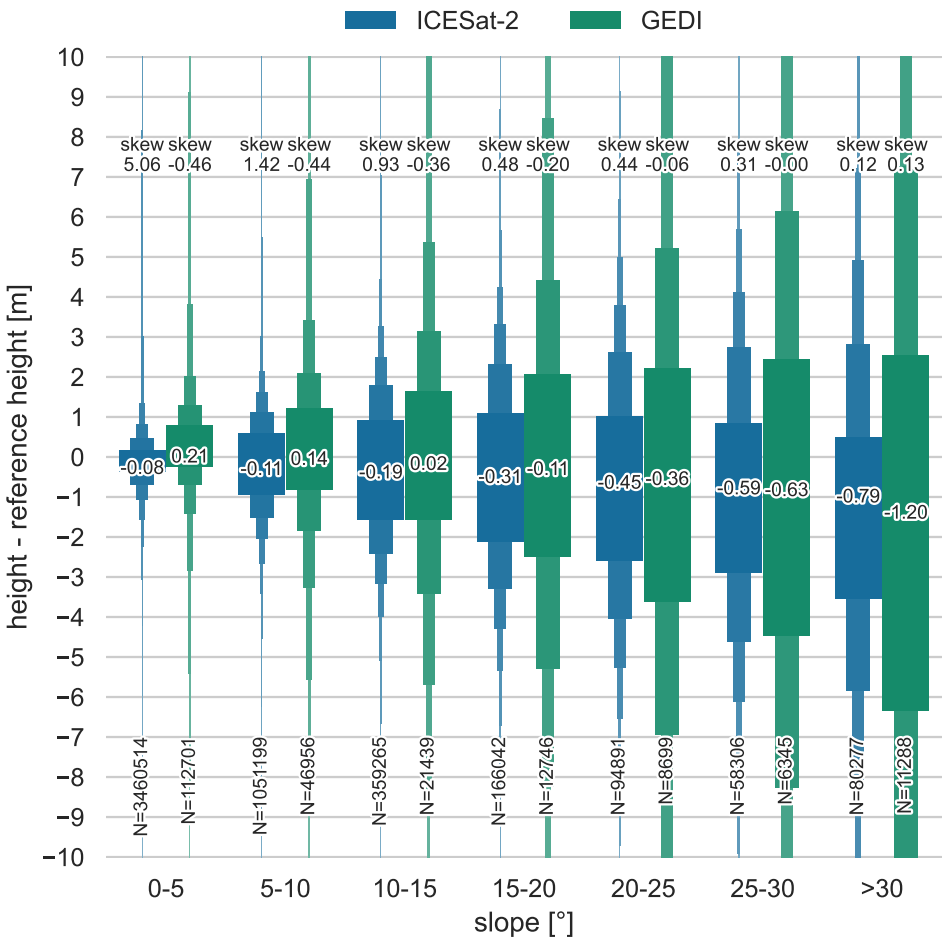

Figure 9: Elevation difference per slope category in Switzerland as boxenplots for both missions compared to reference areas. The skewness, median, and the number of samples is included in the top, middle and lower part of the figure, respectively. Note how an increasing slope has a negative correlation on the accuracy and precision and that GEDI suffers more from this effect than ICESat-2.

onboard resources (Neuenschwander and Pitts, 2019). It would then achieve the same lifespan as ICESat-1 (±5 years). In this optimistic scenario, we would see a sub 500 m resolution everywhere. For achieving even higher resolutions, a constellation of ICESat-2 like satellites was already proposed by Hancock et al. (2021).

4.3. Limitations and overall recommendations

A direct point-to-point comparison between ICESat-2 and GEDI is not straightforward and has not been implemented. As shown in Figure 2 and 10a, the different orbits and beam configurations of the two missions yield few intersections between footprints. After filtering, even fewer points remain, and the number of points is too low to perform an analysis that could relate to environmental factors such as land cover or slope.

In this study we rasterise the ICESat-2 and GEDI samples to assess their spatial coverage, which is an understudied aspect of these sparse datasets. While this gives an upper bound on the resolution of a (global) DEM, we do not seek to create one: it would require more research into combining these two different datasets. Instead, we emphasize that the application of spaceborne lidar is probably more limited by its spatial coverage—depending on the latitude of the area of interest—than its vertical accuracy.

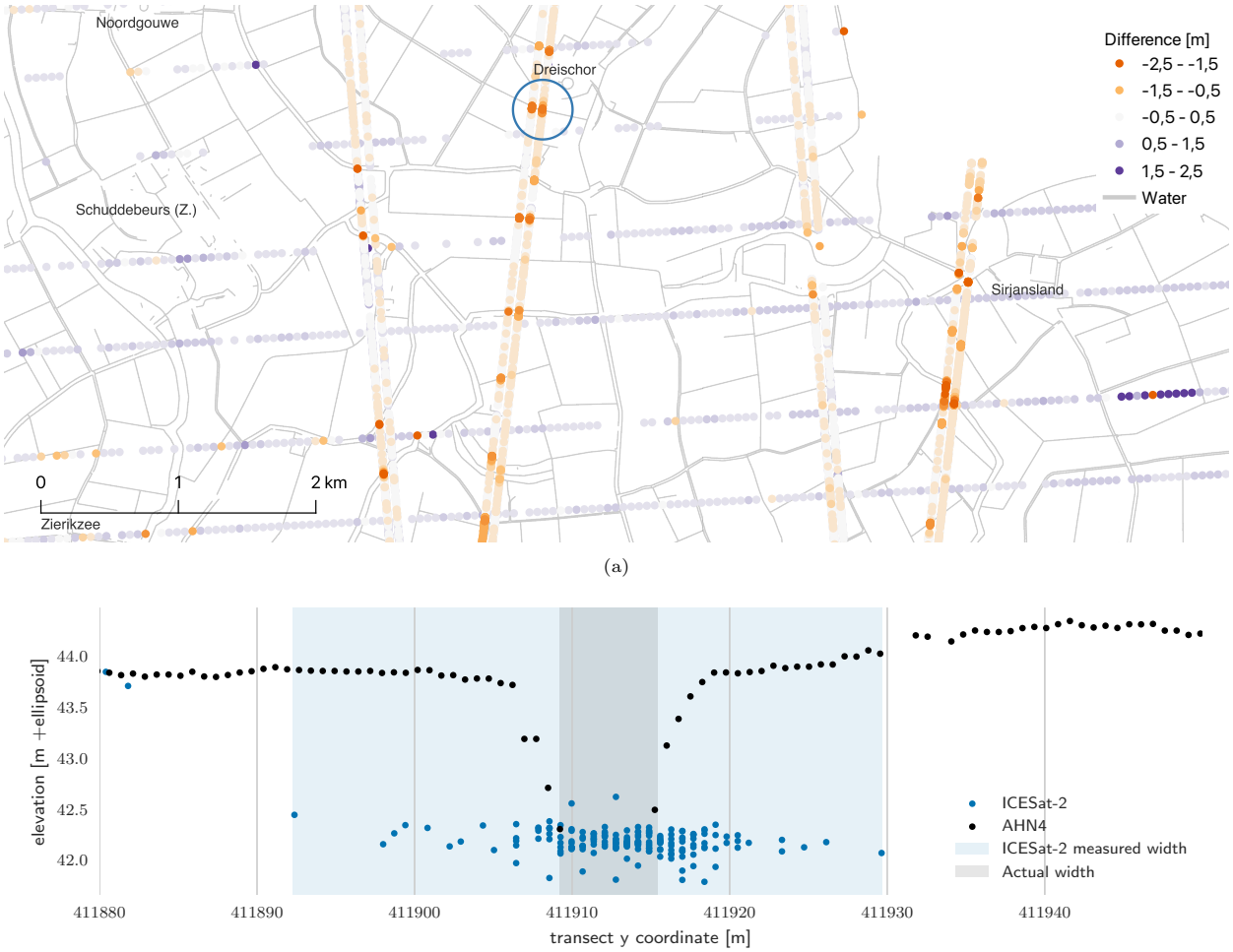

Figure 10: (a) Selection of ICESat-2 and GEDI measurements (not to scale) over Schouwen-Duiveland (near Dreischor and Sirjansland) in the Netherlands, coloured for difference with AHN4. Negative outliers (coloured in orange) most often occur at water bodies (grey lines are rivers, canals, or ditches from TOP10NL). (b) Cross-section of a ditch from (a), indicated with blue circle, with ICESat-2 points and AHN4 as reference. ICESat-2 points—actually ±17 m wide footprints—can exaggerate the width of highly reflective features, such as the water in a ditch. Note the large number of points in the ditch itself as well, indicative of a specular reflection.

For practical purposes, we note that the data sizes involved can hinder processing. This is especially true for GEDI, and while version 2 was improved by dividing each orbit into four granules, the number of granules and total download size exceeds ICESat-2 while having ±100 times fewer data points. Similarly, while the filters applied in this study are effective, they are not straightforward to implement (particularly so for ICESat-2), and incomplete for detecting all outlier tracks. It must be noted that the data products of ICESat-2 and GEDI are still in development and are subject to improvements.

5. Conclusions

In this study, we validated the terrain measurements of ICESat-2 and GEDI lidar satellites against airborne lidar datasets over three areas in the Netherlands, Switzerland and New Zealand. We used three and a half years of ICESat-2 ATL03 data (2018-10-13 to 2022-04-04) and three years of GEDI L2A data (2019-04-18 to 2022-03-16) for a total of 113 million measurements.

For all areas and land cover classes combined, ICESat-2 achieved a bias of −0.06 m, a MAE of 0.46 m, and a RMSE of 1.39 m (N=107 259 203). We found that GEDI is less accurate and precise with a bias of 0.45 m, a MAE of 0.98 and a RMSE of 5.66 (N=6 097 197). The difference in the number of samples stems from the higher sampling rate of ICESat-2 compared to GEDI. Measurements in open land cover classes, such as "Cropland" and "Grassland", result in the best precision for both missions. Precision decreases in "Sparse vegetation" areas and is worst in "Tree Cover" for GEDI and in "Built-up" areas for ICESat-2. Both missions are the least accurate in urban areas, as buildings are mistaken for ground, resulting in a strong positive bias of 0.7 m.

We found that the slope of the measured terrain has a major influence on accuracy, and more so for GEDI than ICESat-2. Based on the decrease in accuracy on sloped terrain, we estimated the horizontal geolocation error of ICESat-2 at 4 m and that of GEDI at 9 m. Overall, little effect of either beam power or day-time of measurements was found, nor did we find significant seasonal effects on accuracy. We concluded that the applied filtering is sufficient to remove most outliers for both products. Our results are comparable or better than previous studies, which we also attribute to using newer versions of the data products.

Furthermore, we investigated the current spatial coverage of ICESat-2 and GEDI by deriving a DEM at different resolutions and latitudes. GEDI has higher spatial coverage than ICESat-2 at lower latitudes, due to its beam pattern and lower inclination angle, and can achieve a resolution of 700 m. ICESat-2 only reaches a resolution of 2000 m at the equator, but increases to almost 200 m at higher latitudes. Finally, we showed that a DEM of 500 m resolution could be achieved when ICESat-2 and GEDI are combined.

We provided recommendations on processing both ICESat-2 and GEDI data for DEM creation, especially in terms of filtering outlier tracks. With these filters applied, both ICESat-2 and GEDI enable accurate terrain measurements anywhere in the world. In data-poor areas with ubiquitous forest cover—such as the tropics—these spaceborne lidar instruments enable accurate remote-sensed terrain measurements for the first time. This has considerable potential for new applications and insights, such as estimation of flood risk.

Appendix A. GEDI filtering

The GEDI data are filtered based on the parameters used for the higher level L3A gridded data product. These parameters are described in section 3.3.1 of the GEDI ATBD document (Dubayah et al., 2021c) and are repeated here in Table A.4

Table A.4: Filter parameters used to filter GEDI. Replication of Table 3-2 in the GEDI ATBD document (Dubayah et al., 2021c) for GEDI L3A.

L2A Variable Name	Criteria for Return Inclusion
rx_assess_quality_flag	!= 0
surface_flag	!= 0
stale_return_flag	== 0
rx_maxamp	>8*sd_corrected
sensitivity	<=1 and >0.90
rx_algrunflag	!= 0
zcross	>0
toploc	>0
degrade_flag	== 0

Appendix B. Overview of validation areas

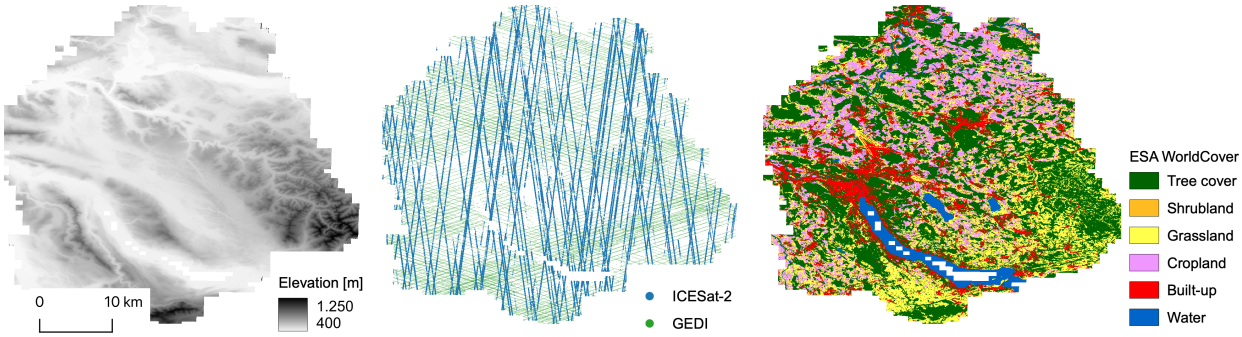

Figure B.11: A visual overview of the datasets used for the reference area in Switzerland.

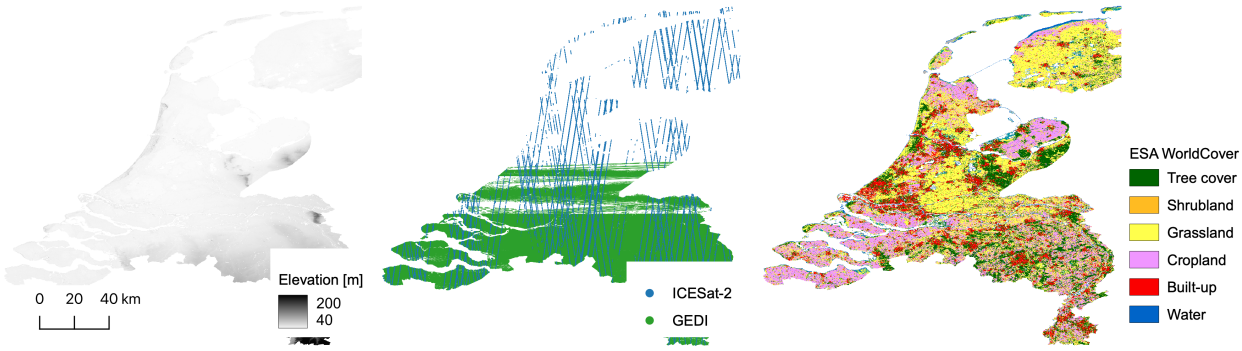

Figure B.12: A visual overview of the datasets used for the reference area in The Netherlands.

Appendix C. Landcover statistics per validation area

Table C.5: Validation with reference areas for each landcover class in The Netherlands

Landcover	bias [m]		MAE [m]		RMSE [m]		number of observations	
	ICESat-2	GEDI	ICESat-2	GEDI	ICESat-2	GEDI	ICESat-2	GEDI
Sparse vegetation	−0.07	0.26	0.41	0.93	1.09	4.25	1 948 454	58 267
Grassland	−0.20	0.29	0.37	0.76	0.79	4.90	57 362 955	2 146 375
Cropland	−0.03	0.38	0.25	0.63	0.56	4.22	21 302 538	1 814 420
Tree cover	−0.20	0.65	0.52	1.15	1.21	6.07	10 734 483	1 150 877
Built-up	0.94	0.81	1.42	1.23	3.33	6.24	8 111 400	554 722
All landcovers	−0.06	0.44	0.44	0.85	1.23	5.10	99 459 830	5 724 661

Table C.6: Validation with reference areas for each landcover class in Switzerland

Landcover	bias [m]		MAE [m]		RMSE [m]		number of observations	
	ICESat-2	GEDI	ICESat-2	GEDI	ICESat-2	GEDI	ICESat-2	GEDI
Sparse vegetation	−0.40	0.56	1.05	3.29	3.44	13.29	48 646	1547
Grassland	−0.13	0.49	0.36	1.95	1.91	10.81	2 126 953	63 514
Cropland	−0.07	0.29	0.28	0.91	1.67	6.38	1 255 387	35 727
Tree cover	−0.19	0.76	0.72	3.81	3.37	13.33	1 307 515	99 617
Built-up	0.92	2.07	1.42	2.82	4.38	16.18	512 176	19 705
All landcovers (slope 0° to 5°)	0.04	0.83	0.42	1.58	2.38	10.15	3 441 930	112 636
All landcovers	−0.03	0.72	0.54	2.70	2.64	12.05	5 250 677	220 110

Table C.7: Validation with reference areas for each landcover class in New Zealand. Note that GEDI has a much higher percentage in tree cover (the worst performing landcover) than ICESat-2, impacting the all landcovers result negatively.

Landcover	bias [m]		MAE [m]		RMSE [m]		number of observations	
	ICESat-2	GEDI	ICESat-2	GEDI	ICESat-2	GEDI	ICESat-2	GEDI
Sparse vegetation	−0.23	−1.26	1.02	3.85	3.13	9.74	55 559	2212
Grassland	−0.07	−0.04	0.39	1.88	1.89	5.05	1 671 689	78 292
Cropland	0.11	0.13	0.40	0.83	2.12	2.37	135 558	5679
Tree cover	0.10	0.63	1.20	6.43	3.96	15.03	384 473	56 669
Built-up	2.32	0.90	2.53	1.43	5.13	3.26	301 417	9574
All landcovers	0.24	0.25	0.78	3.53	2.87	9.98	2 548 696	152 426

Appendix D. Unused granules

The following list contains our unused granules that intersect with the validation areas based on our outlier filtering. This list is thus incomplete for locations outside the validation areas. The list contains 38 granules, 3% of a total of 1488 granules with data after processing 2655 downloaded granules.

- GEDI02_A_2022014225329_O17510_03_T06747_02_003_02_V002

- GEDI02_A_2020025190742_O06347_03_T00718_02_003_01_V002
- GEDI02_A_2022014212037_O17509_02_T11168_02_003_02_V002
- GEDI02_A_2021361060558_O17220_03_T07160_02_003_02_V002
- GEDI02_A_2019338133454_O05537_02_T05261_02_003_01_V002
- GEDI02_A_2021060044323_O12554_03_T09409_02_003_02_V002
- GEDI02_A_2022015220635_O17525_03_T06150_02_003_02_V002
- GEDI02_A_2020025190742_O06347_02_T00718_02_003_01_V002
- GEDI02_A_2022025185520_O17678_03_T11108_02_003_02_V002
- GEDI02_A_2019314030833_O05158_03_T02800_02_003_01_V002
- GEDI02_A_2021060044323_O12554_02_T09409_02_003_02_V002
- GEDI02_A_2022012225425_O17479_02_T09516_02_003_02_V002
- GEDI02_A_2020021204150_O06286_03_T00565_02_003_01_V002
- GEDI02_A_2020333163124_O11120_02_T08062_02_003_02_V002
- GEDI02_A_2019328195621_O05386_03_T05385_02_003_01_V002
- GEDI02_A_2021298064602_O16244_03_T06303_02_003_02_V002
- GEDI02_A_2022011002854_O17449_03_T10863_02_003_02_V002
- GEDI02_A_2020026151521_O06360_04_T00119_02_003_01_V002
- GEDI02_A_2020214160310_O09275_02_T03931_02_003_01_V002
- GEDI02_A_2021308020830_O16396_02_T07496_02_003_02_V002
- GEDI02_A_2021299055944_O16259_02_T09822_02_003_02_V002
- GEDI02_A_2019121050103_O02164_02_T00748_02_003_01_V002
- GEDI02_A_2022013220732_O17494_02_T08919_02_003_02_V002
- GEDI02_A_2020316001737_O10846_03_T08139_02_003_02_V002
- GEDI02_A_2021309012206_O16411_02_T06746_02_003_02_V002
- ATL03_20190319072029_12350202_005_01
- ATL03_20190408063849_01530302_005_01
- ATL03_20211119210143_08921306_005_01
- ATL03_20181115131301_07320102_005_01
- GEDI02_A_2021296064540_O16213_02_T07955_02_003_02_V002
- ATL03_20190718140907_03130406_005_01
- ATL03_20190306081109_10370202_005_01
- ATL03_20211002111700_01531302_005_01

- ATL03_20210604170058_10981102_005_01
- ATL03_20200224150648_09150602_005_01
- ATL03_20191009100549_01910506_005_01
- ATL03_20211019101803_04121302_005_01
- ATL03_20191022091513_03890506_005_01

All these granules consistently exceed the reference surface, included in the products themselves, by more than 30 m on average. We noted that all GEDI outlier tracks are consistently above the reference surface, while the ICESat-2 outliers are more balanced, but mostly below the reference surface.

References

Adam, M., Urbazaev, M., Dubois, C., Schmullius, C., 2020. Accuracy Assessment of GEDI Terrain Elevation and Canopy Height Estimates in European Temperate Forests: Influence of Environmental and Acquisition Parameters. Remote Sensing 12, 3948. doi:10.3390/rs12233948.

Bates, P.D., 2012. Integrating remote sensing data with flood inundation models: How far have we got? Hydrological Processes 26, 2515–2521. doi:10/ghq4wd.

Bezanson, J., Edelman, A., Karpinski, S., Shah, V.B., 2017. Julia: A Fresh Approach to Numerical Computing. SIAM Rev. 59, 65–98. doi:10/f9wkpj.

van Dijk, A., Bos, M.G., 2013. GIS and Remote Sensing Techniques in Land- and Water-management. Springer Science & Business Media.

Dubayah, R., Blair, J.B., Goetz, S., Fatoyinbo, L., Hansen, M., Healey, S., Hofton, M., Hurtt, G., Kellner, J., Luthcke, S., Armston, J., Tang, H., Duncanson, L., Hancock, S., Jantz, P., Marselis, S., Patterson, P.L., Qi, W., Silva, C., 2020. The Global Ecosystem Dynamics Investigation: High-resolution laser ranging of the Earth's forests and topography. Science of Remote Sensing 1, 100002. doi:10/ggjxx8.

Dubayah, R., Hofton, M., Blair, J., Armston, J., Tang, H., Luthcke, S., 2021a. GEDI L2A Elevation and Height Metrics Data Global Footprint Level V002 (User Guide). doi:10.5067/GEDI/GEDI02_A.002.

Dubayah, R., Luthcke, S., Sabaka, T., Nicholas, J., Preaux, S., Hofton, M., 2021b. GEDI L3 gridded land surface metrics, version 1 doi:10/gjn6fv.

Dubayah, R.O., Luthcke, S.B., Sabaka, T.J., Nicholas, J.B., Preaux, S., Hofton, M.A., 2021c. GEDI L3 Gridded Land Surface Metrics, Version 2. ORNL DAAC doi:10.3334/ORNLDAAC/1952.

Funning, G.J., Parsons, B., Wright, T.J., Jackson, J.A., Fielding, E.J., 2005. Surface displacements and source parameters of the 2003 Bam (Iran) earthquake from Envisat advanced synthetic aperture radar imagery. Journal of Geophysical Research: Solid Earth 110. doi:10.1029/2004JB003338.

Hancock, S., McGrath, C., Lowe, C., Davenport, I., Woodhouse, I., 2021. Requirements for a Global Lidar System: Spaceborne lidar with wall-to-wall coverage. Royal Society Open Science .

Hengl, T., Leal Parente, L., Krizan, J., Bonannella, C., 2020. Continental Europe Digital Terrain Model at 30 m resolution based on GEDI, ICESat-2, AW3D, GLO-30, EUDEM, MERIT DEM and background layers. doi:10.5281/zenodo.4724549.

Hofmann, H., Wickham, H., Kafadar, K., 2017. Letter-Value Plots: Boxplots for Large Data. Journal of Computational and Graphical Statistics 26, 469–477. doi:10/gf38v7.

Hooijer, A., Vernimmen, R., 2021. Global LiDAR land elevation data reveal greatest sea-level rise vulnerability in the tropics. Nat Commun 12, 3592. doi:10/gkzf49.

Liu, A., Cheng, X., Chen, Z., 2021. Performance evaluation of GEDI and ICESat-2 laser altimeter data for terrain and canopy height retrievals. Remote Sensing of Environment 264, 112571. doi:10/gkzw4v.

Luthcke, S.B., Thomas, T.C., Pennington, T.A., Rebold, T.W., Nicholas, J.B., Rowlands, D.D., Gardner, A.S., Bae, S., 2021. ICESat-2 Pointing Calibration and Geolocation Performance. Earth and Space Science 8, e2020EA001494. doi:10.1029/2020EA001494.

Magruder, L., Neuenschwander, A., Klotz, B., 2021. Digital terrain model elevation corrections using space-based imagery and ICESat-2 laser altimetry. Remote Sensing of Environment 264, 112621. doi:10/gmhzpq.

Malambo, L., Popescu, S.C., 2021. Assessing the agreement of ICESat-2 terrain and canopy height with airborne lidar over US ecozones. Remote Sensing of Environment 266, 112711. doi:10/gmxn3k.

Mallet, C., Bretar, F., 2009. Full-waveform topographic lidar: State-of-the-art. ISPRS Journal of Photogrammetry and Remote Sensing 64, 1–16. doi:10.1016/j.isprsjprs.2008.09.007.

Markus, T., Neumann, T., Martino, A., Abdalati, W., Brunt, K., Csatho, B., Farrell, S., Fricker, H., Gardner, A., Harding, D., Jasinski, M., Kwok, R., Magruder, L., Lubin, D., Luthcke, S., Morison, J., Nelson, R., Neuenschwander, A., Palm, S., Popescu, S., Shum, CK., Schutz, B.E., Smith, B., Yang, Y., Zwally, J., 2017. The Ice, Cloud, and land Elevation Satellite-2 (ICESat-2): Science requirements, concept, and implementation. Remote Sensing of Environment 190, 260–273. doi:10/gg3f7c.

Masoud, A.A., Koike, K., 2011. Auto-detection and integration of tectonically significant lineaments from SRTM DEM and remotely-sensed geophysical data. ISPRS Journal of Photogrammetry and Remote Sensing 66, 818–832. doi:10.1016/j.isprsjprs.2011.08.003.

Meigs, A., 2013. Active tectonics and the LiDAR revolution. Lithosphere 5, 226–229. doi:10.1130/RF.L004.1.

Moudry, V., Lecours, V., Gdulová, K., Gábor, L., Moudrá, L., Kropáček, J., Wild, J., 2018. On the use of global DEMs in ecological modelling and the accuracy of new bare-earth DEMs. Ecological Modelling 383, 3–9. doi:10.1016/j.ecolmodel.2018.05.006.

Neuenschwander, A., Guenther, E., White, J.C., Duncanson, L., Montesano, P., 2020. Validation of ICESat-2 terrain and canopy heights in boreal forests. Remote Sensing of Environment 251, 112110. doi:10/ghdkrh.

Neuenschwander, A., Pitts, K., 2019. The ATL08 land and vegetation product for the ICESat-2 Mission. Remote Sensing of Environment 221, 247–259. doi:10/gf9wmm.

Neuenschwander, A.L., Magruder, L.A., 2019. Canopy and Terrain Height Retrievals with ICESat-2: A First Look. Remote Sensing 11, 1721. doi:10/gf9wmn.

Neuenschwander, A.L., Pitts, K.L., Jelley, B.P., Robbins, J., Klotz, B., Popescu, S.C., Nelson, R.F., Harding, D., Pederson, D., Sheridan, R., 2021. ATLAS/ICESat-2 L3A Land and Vegetation Height, version 5. doi:10.5067/ATLAS/ATL08.005.

Neumann, T.A., Brenner, A., Hancock, D., Robbins, J., Saba, J., Harbeck, K., Gibbons, A., Lee, J., Luthcke, S.B., Rebold, T., 2021. ATLAS/ICESat-2 L2A Global Geolocated Photon Data, version 5. doi:10.5067/ATLAS/ATL03.005.

Neumann, T.A., Martino, A.J., Markus, T., Bae, S., Bock, M.R., Brenner, A.C., Brunt, K.M., Cavanaugh, J., Fernandes, S.T., Hancock, D.W., Harbeck, K., Lee, J., Kurtz, N.T., Luers, P.J., Luthcke, S.B., Magruder, L., Pennington, T.A., Ramos-Izquierdo, L., Rebold, T., Skoog, J., Thomas, T.C., 2019. The Ice, Cloud, and Land Elevation Satellite – 2 mission: A global geolocated photon product derived from the Advanced Topographic Laser Altimeter System. Remote Sensing of Environment 233, 111325. doi:10/ghf8jm.

Okolie, C.J., Smit, J.L., 2022. A systematic review and meta-analysis of Digital elevation model (DEM) fusion: Pre-processing, methods and applications. ISPRS Journal of Photogrammetry and Remote Sensing 188, 1–29. doi:10.1016/j.isprsjprs.2022.03.016.

Pronk, M., Gardner, A., 2021. SpaceLiDAR.jl. Zenodo. doi:10.5281/zenodo.7527509.

Quiros, E., Polo, M.E., Fragoso-Campon, L., 2021. GEDI Elevation Accuracy Assessment: A Case Study of Southwest Spain. IEEE Journal of Selected Topics in Applied Earth Observations and Remote Sensing , 1–1doi:10/gj6rvq.

Schneider, F.D., Ferraz, A., Hancock, S., Duncanson, L.I., Dubayah, R.O., Pavlick, R.P., Schimel, D.S., 2020. Towards mapping the diversity of canopy structure from space with GEDI. Environ. Res. Lett. 15, 115006. doi:10/gg27d9.

Schumann, G.J.P., Bates, P.D., 2018. The Need for a High-Accuracy, Open-Access Global DEM. Frontiers in Earth Science 6, 225. doi:10/gnjm7j.

Shen, X., Ke, C.Q., Fan, Y., Drolma, L., 2021. A fine-scale digital elevation model of Antarctica derived from ICESat-2. The Cryosphere Discussions , 1–21.

Sidik, S.M., 2022. Scientists Fight to Keep Lidar on the Space Station. Eos 103.

Su, J., Bork, E., 2006. Influence of Vegetation, Slope, and Lidar Sampling Angle on DEM Accuracy. Photogrammetric Engineering & Remote Sensing 72, 1265–1274. doi:10.14358/PERS.72.11.1265.

Thuillier, G., Hersé, M., Labs, D., Foujols, T., Peetermans, W., Gillotay, D., Simon, P., Mandel, H., 2003. The Solar Spectral Irradiance from 200 to 2400 nm as Measured by the SOLSPEC Spectrometer from the Atlas and Eureca Missions. Solar Physics 214, 1–22. doi:10.1023/A:1024048429145.

Urbazaev, M., Hess, L.L., Hancock, S., Sato, L.Y., Ometto, J.P., Thiel, C., Dubois, C., Heckel, K., Urban, M., Adam, M., Schmullius, C., 2022. Assessment of terrain elevation estimates from ICESat-2 and GEDI spaceborne LiDAR missions across different land cover and forest types. Science of Remote Sensing 6, 100067. doi:10.1016/j.srs.2022.100067.

Vernimmen, R., Hooijer, A., 2023. New LiDAR-Based Elevation Model Shows Greatest Increase in Global Coastal Exposure to Flooding to Be Caused by Early-Stage Sea-Level Rise. Earth's Future 11, e2022EF002880. doi:10.1029/2022EF002880.

Wake, S., Ramos-Izquierdo, L.A., Eegholm, B., Dogoda, P., Denny, Z., Hersh, M., Mulloney, M., Thomes, W.J., Ott, M.N., Jakeman, H., Poulios, D., Mule, P., de Leon, E., Blair, J.B., 2019. Optical system design and integration of the Global Ecosystem Dynamics Investigation Lidar, in: Infrared Remote Sensing and Instrumentation XXVII, SPIE. pp. 99–111. doi:10.1117/12.2530653.

Wang, C., Wang, C., Wang, C., Zhu, X., Zhu, X., Zhu, X., Nie, S., Nie, S., Nie, S., Xi, X., Li, D., Zheng, W., Chen, S., 2019. Ground elevation accuracy verification of ICESat-2 data: A case study in Alaska, USA. Opt. Express, OE 27, 38168–38179. doi:10/ggtqmg.

Xing, Y., Huang, J., Gruen, A., Qin, L., 2020. Assessing the Performance of ICESat-2/ATLAS Multi-Channel Photon Data for Estimating Ground Topography in Forested Terrain. Remote Sensing 12, 2084. doi:10.3390/rs12132084.

Yang, L., Meng, X., Zhang, X., 2011. SRTM DEM and its application advances. International Journal of Remote Sensing 32, 3875–3896. doi:10.1080/01431161003786016.

Zanaga, D., Van De Kerchove, R., De Keersmaecker, W., Souverijns, N., Brockmann, C., Quast, R., Wevers, J., Grosu, A., Paccini, A., Vergnaud, S., Cartus, O., Santoro, M., Fritz, S., Georgieva, I., Lesiv, M., Carter, S., Herold, M., Li, L., Tsendbazar, Nandin-Erdene, Ramoino, F., Arino, O., 2021. ESA WorldCover 10 m 2020 v100. doi:10.5281/ZENODO.5571936.

Zhao, P., Li, S., Ma, Y., Liu, X., Yang, J., Yu, D., 2022. A new terrain matching method for estimating laser pointing and ranging systematic biases for spaceborne photon-counting laser altimeters. ISPRS Journal of Photogrammetry and Remote Sensing 188, 220–236. doi:10.1016/j.isprsjprs.2022.04.015.

Zhu, X., Nie, S., Wang, C., Xi, X., Hu, Z., 2018. A Ground Elevation and Vegetation Height Retrieval Algorithm Using Micro-Pulse Photon-Counting Lidar Data. Remote Sensing 10, 1962. doi:10.3390/rs10121962.